

# Impedance-based Gaussian Processes for Predicting Human Behavior during Physical Interaction

José Ramón Medina, Satoshi Endo and Sandra Hirche

**Abstract**—For seamless physical human-robot interaction (pHRI), a prediction about the human motion intention is essential. Typically, most system identification approaches to pHRI model the human as a black box without prior assumptions about the underlying behavioral structure. However, integrating a priori knowledge about human behavior provides better prediction performance and its generalization capability. Thus, we present a novel method for human intention estimation using Gaussian Processes (GP) on an empirically supported human motor control model. In this article, the arm dynamics of a human is modeled as mechanical impedance which tracks a latent desired trajectory. We then adopt a Bayesian perspective by assuming GP priors on impedance parameters and the desired trajectory, which allows regression about the human motion intention from observed interaction forces. The proposed impedance-based GP model is validated in an experiment with human users to demonstrate its prediction performance.

## I. INTRODUCTION

The advancements of technologies have led to global expectations for robotic systems to engage in physical human-robot interaction (pHRI), and assist a user in industrial and domestic applications. The physical coupling between a human and a robot imposes unique constraints to efficient and safe control of a robot as a mismatched motion plan could directly perturb the human partner. Thus, estimating underlying human motion intention with which the robot coordinates its motion is a key to successful pHRI.

In applications, a behavioral model of a human is typically treated as a 'black box' where inputs (e.g., human body configuration) and outputs (e.g., interaction force) are deterministically or stochastically mapped as a parametric model, for instance, in Programming by Demonstration (PbD) [1] [2]. In this type of modeling techniques, interaction behavior is encoded into a probabilistic model, capturing the joint statistics of observed trajectories and associated interaction forces [1] [3] [4]. While stochastic methods based on naïve models are relatively easy to implement, they suffer from limited expressiveness. For example, Gaussian Processes (GP)s are powerful non-parametric model for approximating dynamical systems [5] [6] [7] that only requires the definition of the second-order statistics between function values. However, if the statistics are not defined in accordance with the real function, the rate of convergence may increase exponentially, and no prediction is guaranteed in previously unobserved regions of the input space [8]. This

issue is particularly cumbersome in realistic pHRI when the movements of a human and the robot are loosely defined so their interaction is not guaranteed as repetitive. One way to overcome such limitation is to perform GP regression on a underlying behavioral model of a human to approximate the lower dimensional manifold of human behavior. For instance, research shows the quality of a latent desired trajectory by the human central nervous system (CNS) is regulated by an impedance control scheme [9]. The dynamics of the arm is regulated by contractions of antagonistic pairs of muscles, the stretch reflex and intrinsic viscoelastic properties of the limb in order to optimally follow a latent trajectory [10]. Exploiting such knowledge about underlying human motor control models on system identification remains an open issue with great potential benefits for the prediction performance.

In this work, we present a novel method for human motion prediction using GP on an empirically supported human motor control model. The arm dynamics of a human is modeled as mechanical impedance which tracks a latent desired trajectory. We then adopt a Bayesian perspective by assuming GP priors on impedance parameters and the desired trajectory, which allows regression about the human motion intention from observed interaction forces. The proposed impedance-based GP model is validated in an experiment with human users to demonstrate its prediction performance.

The remainder of this article is structured as follows. The considered problem is formally defined in Section II. A background on GPs is presented in Section III. The proposed impedance-based GP model is presented in Section IV. The model is then validated and evaluated in Section V.

**Notation:** by convention, bold characters are used for vectors and capital letters denote matrices. The expression  $\mathcal{N}(x|\mu, \sigma)$  describes a Gaussian random variable defined over  $x$  with mean  $\mu$  and covariance  $\sigma$ .  $E[x]$  and  $\text{Var}[x]$  denote expected value and variance of  $x$  respectively.  $\mathbb{N}^+$  is a natural positive integer.

## II. PROBLEM SETTING

This work considers an acquisition of a human behavior model when he/she physically interacts with a robot using its force and position sensors at the end-effector. By assuming that the human arm comprises 7 degrees of freedom (DoF), the rigid body dynamics of the arm when tightly grasping the robot end-effector are given by

$$\tau_h + \tau_{\text{int}} = M_q(q)\ddot{q} + C(q, \dot{q})\dot{q} + g(q), \quad (1)$$

where  $q \in \mathbb{R}^7$  is the 7 DoF arm configuration in joint space,  $M_q(q) \in \mathbb{R}^{7 \times 7}$  is the arm inertia ma-

Authors are with the Chair of Information-Oriented Control, Department of Electrical Engineering and Information Technology, Technische Universität München, D-80290 Munich, Germany. {medina, endo, hirche}@tum.de

trix,  $C(\mathbf{q}, \dot{\mathbf{q}})\dot{\mathbf{q}} \in \mathbb{R}^7$  represents the Coriolis and centrifugal forces,  $\mathbf{g}(\mathbf{q}) \in \mathbb{R}^7$  is the gravity vector,  $\boldsymbol{\tau}_h \in \mathbb{R}^7$  is the human joint torque applied and  $\boldsymbol{\tau}_{\text{int}} \in \mathbb{R}^{7 \times 7}$  is the interaction torque resulting from the physical coupling to the robot. The wrench measured at the robot's end-effector  $\mathbf{u}_{\text{int}} \in \mathbb{R}^6$  represents the interaction torque as  $\boldsymbol{\tau}_{\text{int}} = -J(\mathbf{q})^T \mathbf{u}_{\text{int}}$ , where  $J(\mathbf{q})$  is the Jacobian matrix.

The joint torque applied by the human is composed of a feedforward term  $\boldsymbol{\tau}_{\text{FF}}$  and a feedback term  $\boldsymbol{\tau}_{\text{FB}}$  that are subject to neural noise  $\boldsymbol{\varepsilon}_{\boldsymbol{\tau},q}$ , i.e.

$$\boldsymbol{\tau}_h = \boldsymbol{\tau}_{\text{FF}} + \boldsymbol{\tau}_{\text{FB}} + \boldsymbol{\varepsilon}_{\boldsymbol{\tau},q}. \quad (2)$$

The feedforward term represents the inverse dynamics of the musculoskeletal system and interaction dynamics learned by the CNS [11], and it specifies joint torques for attaining a desired trajectory. We assume the desired trajectory is a twice differentiable well-defined function  $\mathbf{q}_d(\boldsymbol{\theta}) : \mathbb{R}^n \rightarrow \mathbb{R}^7$  where  $\boldsymbol{\theta} \in \mathbb{R}^n$  is a task-specific input parameter such as the arm configuration in the present case. Thus, the joint torque specified by the feedforward term is expressed as

$$\begin{aligned} \boldsymbol{\tau}_{\text{FF}} = & \hat{M}_q(\mathbf{q}_d(\boldsymbol{\theta}))\ddot{\mathbf{q}}_d(\boldsymbol{\theta}) + \hat{C}(\mathbf{q}_d(\boldsymbol{\theta}), \dot{\mathbf{q}}_d(\boldsymbol{\theta}))\dot{\mathbf{q}}_d(\boldsymbol{\theta}) \\ & + \hat{\mathbf{g}}(\mathbf{q}_d(\boldsymbol{\theta})) + \hat{\boldsymbol{\tau}}_{\text{int}}(\mathbf{q}, \dot{\mathbf{q}}, \ddot{\mathbf{q}}, \boldsymbol{\theta}), \end{aligned} \quad (3)$$

where  $\hat{\boldsymbol{\tau}}_{\text{int}}(\mathbf{q}, \dot{\mathbf{q}}, \ddot{\mathbf{q}}, \boldsymbol{\theta})$  is the interaction torque estimated by the human, which is a function of the arm configuration and task-specific parameters.

The feedback term compensates small perturbations and generates restoring force towards the desired trajectory. It has been modeled with a Proportional-Derivative (PD) control [11]

$$\boldsymbol{\tau}_{\text{FB}} = D_q(\mathbf{q}, \dot{\mathbf{q}}, \boldsymbol{\theta})(\dot{\mathbf{q}}_d(\boldsymbol{\theta}) - \dot{\mathbf{q}}) + K_q(\mathbf{q}, \dot{\mathbf{q}}, \boldsymbol{\theta})(\mathbf{q}_d(\boldsymbol{\theta}) - \mathbf{q}), \quad (4)$$

where  $K_q(\mathbf{q}, \dot{\mathbf{q}}, \boldsymbol{\theta}), D_q(\mathbf{q}, \dot{\mathbf{q}}, \boldsymbol{\theta}) \in \mathbb{R}^{7 \times 7}$  are configuration, velocity and task-dependent stiffness and damping matrices, respectively.

Substituting (2), (3) and (4) into (1), the interaction torque is given by

$$\begin{aligned} \boldsymbol{\tau}_{\text{int}}(\mathbf{q}, \dot{\mathbf{q}}, \ddot{\mathbf{q}}, \boldsymbol{\theta}) = & M_q(\mathbf{q})\ddot{\mathbf{e}}_q(\boldsymbol{\theta}, \mathbf{q}) + D_q(\mathbf{q}, \dot{\mathbf{q}}, \boldsymbol{\theta})\dot{\mathbf{e}}_q(\boldsymbol{\theta}, \mathbf{q}) \\ & + K_q(\mathbf{q}, \dot{\mathbf{q}}, \boldsymbol{\theta})\mathbf{e}_q(\boldsymbol{\theta}, \mathbf{q}) + \hat{\boldsymbol{\tau}}_{\text{int}}(\mathbf{q}, \dot{\mathbf{q}}, \ddot{\mathbf{q}}, \boldsymbol{\theta}) \\ & + \boldsymbol{\varepsilon}_{\text{dyn},q}(\mathbf{q}, \dot{\mathbf{q}}, \ddot{\mathbf{q}}, \boldsymbol{\theta}) + \boldsymbol{\varepsilon}_{\boldsymbol{\tau},q}, \end{aligned} \quad (5)$$

where  $\mathbf{e}_q(\boldsymbol{\theta}, \mathbf{q}) = \mathbf{q}_d(\boldsymbol{\theta}) - \mathbf{q}$  and  $\boldsymbol{\varepsilon}_{\text{dyn},q}(\bar{\boldsymbol{\xi}})$  represent feedforward specification errors about the dynamics of own body and the environment. From (5), the interaction dynamics in the task space are given by

$$\begin{aligned} -\mathbf{u}_{\text{int}}(\bar{\boldsymbol{\xi}}) = & M(\mathbf{x})\ddot{\mathbf{e}}(\boldsymbol{\theta}, \mathbf{x}) + D(\boldsymbol{\xi})\dot{\mathbf{e}}(\boldsymbol{\theta}, \mathbf{x}) + K(\boldsymbol{\xi})\mathbf{e}(\boldsymbol{\theta}, \mathbf{x}) \\ & + \hat{\mathbf{u}}_{\text{int},\varepsilon}(\bar{\boldsymbol{\xi}}) + \boldsymbol{\varepsilon}_{\boldsymbol{\tau}}, \end{aligned} \quad (6)$$

where  $\mathbf{x} \in \mathbb{R}^6$  is the human hand configuration which follows from the forward kinematics mapping  $L(\mathbf{q}) : \mathbb{R}^7 \rightarrow \mathbb{R}^6$ ,  $\mathbf{e}(\boldsymbol{\theta}, \mathbf{x}) = \mathbf{x}_d(\boldsymbol{\theta}) - \mathbf{x}$ ,

where  $\mathbf{x}_d(\boldsymbol{\theta})$  is the human desired trajectory in task space,  $\boldsymbol{\xi} = [\mathbf{x}^T \dot{\mathbf{x}}^T \ddot{\mathbf{x}}^T \boldsymbol{\theta}^T]^T$  and  $\bar{\boldsymbol{\xi}} = [\mathbf{x}^T \dot{\mathbf{x}}^T \ddot{\mathbf{x}}^T \boldsymbol{\theta}^T]^T$  and

$$M(\mathbf{x}) = J(\mathbf{q})^{-T} M_q(\mathbf{q}) J(\mathbf{q})^{-1}$$

$$D(\boldsymbol{\xi}) = J(\mathbf{q})^{-T} D_q(\mathbf{q}, \dot{\mathbf{q}}, \boldsymbol{\theta}) J(\mathbf{q})^{-1}$$

$$K(\boldsymbol{\xi}) = J(\mathbf{q})^{-T} K_q(\mathbf{q}, \dot{\mathbf{q}}, \boldsymbol{\theta}) J(\mathbf{q})^{-1}$$

$$\boldsymbol{\varepsilon}_{\boldsymbol{\tau}} = J(\mathbf{q})^{-T} \boldsymbol{\varepsilon}_{\boldsymbol{\tau},q}$$

$$\hat{\mathbf{u}}_{\text{int},\varepsilon}(\bar{\boldsymbol{\xi}}) = J(\mathbf{q})^{-T} (\hat{\boldsymbol{\tau}}_{\text{int}}(\mathbf{q}, \dot{\mathbf{q}}, \ddot{\mathbf{q}}, \boldsymbol{\theta}) + \boldsymbol{\varepsilon}_{\text{dyn},q}(\mathbf{q}, \dot{\mathbf{q}}, \ddot{\mathbf{q}}, \boldsymbol{\theta})).$$

Given observations  $\{\bar{\boldsymbol{\xi}}, \mathbf{u}_{\text{int}}\}$  from physical interaction, the present work estimates  $\mathbf{u}_{\text{int}}(\bar{\boldsymbol{\xi}})$ , assuming the interaction dynamics as defined in (6).

### III. GAUSSIAN PROCESS PRIORS

A GP  $f(\boldsymbol{\xi})$ , with  $\mathbf{z} \in \mathbb{R}^n$  and  $f(\mathbf{z}) : \mathbb{R}^n \rightarrow \mathbb{R}$ , is a statistical distribution over function values where any finite collection of samples  $\{f(\mathbf{z}_1) \cdots f(\mathbf{z}_h)\}$ , with  $h \in \mathbb{N}^+$ , forms a multivariate Gaussian random variable. Thus, a GP is fully defined by its mean

$$m(\mathbf{z}) = \mathbb{E}[f(\mathbf{z})]$$

and covariance function

$$\begin{aligned} k(\mathbf{z}, \mathbf{z}') = & \text{Cov}[\Delta f(\mathbf{z}), \Delta f(\mathbf{z}')] \\ = & \mathbb{E}[(f(\mathbf{z}) - m(\mathbf{z}))(f(\mathbf{z}') - m(\mathbf{z}'))^T]. \end{aligned}$$

The definition of  $f(\mathbf{z})$  as a GP is compactly formulated as  $f(\mathbf{z}) \sim \mathcal{GP}(m(\mathbf{z}), k(\mathbf{z}, \mathbf{z}'))$ .

GPs benefit from the desirable properties of multivariate normal distributions. The joint prior distribution of a given training set of noisy observations  $\mathbf{y} = \{y_i\}_{i=1}^h$  at input points  $Z = \{\mathbf{z}_i\}_{i=1}^h$  and predictive output  $y_*$  at test input  $\mathbf{z}_*$  is

$$\begin{aligned} \mathbb{P}(\mathbf{y}, y_* | Z, \mathbf{z}_*) = & \\ = & \mathcal{N}\left(\begin{bmatrix} \mathbf{y} \\ y_* \end{bmatrix} \middle| \begin{bmatrix} m(Z) \\ m(\mathbf{z}_*) \end{bmatrix}, \begin{bmatrix} K + \sigma_n^2 I & \mathbf{k}_* \\ \mathbf{k}_*^T & k_{**} + \sigma_n^2 \end{bmatrix}\right), \end{aligned}$$

where  $\mathbf{k}_* = k(\mathbf{z}_*, Z)$ ,  $k_{**} = k(\mathbf{z}_*, \mathbf{z}_*)$  and  $K = k(Z, Z)$  and  $\sigma_n^2$  is the observation noise variance. By means of multivariate Gaussian conditioning, i.e. applying Bayes' rule, the conditional (predictive) posterior is defined as

$$\begin{aligned} \mathbb{P}(y_* | \mathbf{y}, Z, \mathbf{z}_*) = & \\ \mathcal{N}(y_* | m(\boldsymbol{\xi}_*), & + \mathbf{k}_*^T K^{-1} \mathbf{y}, \sigma_n^2 + k_{**} - \mathbf{k}_*^T (K + \sigma_n^2 I)^{-1} \mathbf{k}_*). \end{aligned} \quad (7)$$

The computational load of this expression is governed by matrix inversion  $(K + \sigma_n^2 I)^{-1}$  with complexity  $\mathcal{O}(h^3)$ . The application of GPs in realistic scenarios requires sparse or local approximations.

### IV. BAYESIAN IMPEDANCE MODEL

In order to obtain an estimate of (6) from pHRI data, we adopt a Bayesian framework by assuming prior distributions on unknown latent variables. For simplicity and tractability we neglect biomechanical constraints by considering  $M(\mathbf{x})$ ,  $D(\boldsymbol{\xi})$  and  $K(\boldsymbol{\xi})$  diagonal matrices such that interaction force exerted on the  $i$ -th dimension is

$$u_{\text{int}}(\bar{\xi}) = u_{\text{imp}}(\bar{\xi}) + \hat{u}_{\text{int},\varepsilon}(\bar{\xi}) + \varepsilon_\tau \quad (8)$$

with

$$u_{\text{imp}}(\bar{\xi}) = m\ddot{e}(\theta, x_i) + d(\xi)\dot{e}(\theta, x_i) + k(\xi)e(\theta, x_i), \quad (9)$$

where  $u_{\text{int}}(\bar{\xi})$ ,  $\hat{u}_{\text{int},\varepsilon}(\bar{\xi})$ ,  $d(\xi)$ ,  $k(\xi)$ ,  $e(\theta, x_i) = x_d(\theta) - x_i$  and  $x_d(\theta)$  are now one-dimensional functions,  $m$  is a one-dimensional variable and  $\varepsilon_\tau \sim \mathcal{N}(\varepsilon | 0, \sigma_\tau^2)$ . For clarity, the index  $i$  will be omitted from here on in the functionals  $e$ ,  $u_{\text{int}}$ ,  $d$ ,  $k$ ,  $x_d$  and  $\hat{u}_{\text{int}}$ .

### A. Priors

For statistical analysis of (8), we assume that functionals  $d(\xi)$ ,  $k(\xi)$ ,  $x_d(\theta)$  and  $\hat{u}_{\text{int},\varepsilon}(\bar{\xi})$  and variable  $m$  are statistically independent and have prior distributions

$$\begin{aligned} m &\sim \mathcal{N}(m | \mu_m, \sigma_m^2) \\ d(\xi) &\sim \mathcal{GP}(\mu_d, k_d(\xi, \xi')) \\ k(\xi) &\sim \mathcal{GP}(\mu_k, k_k(\xi, \xi')) \\ x_d(\theta) &\sim \mathcal{GP}(\mu_{x_d}, k_{x_d}(\theta, \theta')) \\ \hat{u}_{\text{int},\varepsilon}(\bar{\xi}) &\sim \mathcal{GP}(0, k_{\hat{u}_{\text{int},\varepsilon}}(\bar{\xi}, \bar{\xi}')), \end{aligned} \quad (10)$$

where  $\mu_m$ ,  $\mu_d$  and  $\mu_k$  are the expected mass, damping and stiffness coefficients, respectively.  $\mu_{x_d}$  is the expected desired hand position and  $k_{x_d}(\theta, \theta')$  is a twice differentiable covariance function. For simplicity we do not strictly ensure positivity of  $m$ ,  $d(\xi)$  and  $k(\xi)$ <sup>1</sup>, but probabilistically assumed.

### B. Impedance, PD and interaction force kernels

Given priors (10), a second-order statistical characterization of  $u_{\text{int}}(\bar{\xi})$  entails only complication in the impedance term. Although not Gaussian due to the products involved<sup>2</sup>, the computation of its expected value and the covariance allows its approximation as a GP, i.e.,

$$u_{\text{imp}}(\bar{\xi}) \sim \mathcal{GP}\left(\mathbb{E}[u_{\text{imp}}(\bar{\xi})], k_{\text{imp}}(\bar{\xi}, \bar{\xi}')\right).$$

From (9) and (10) the expected value is

$$\mathbb{E}[u_{\text{imp}}(\bar{\xi})] = \mu_m(\ddot{\mu}_{x_d} - \ddot{x}_i) + \mu_d(\dot{\mu}_{x_d} - \dot{x}_i) + (\mu_{x_d} - x_i). \quad (11)$$

The expression for covariance

$$\begin{aligned} k_{\text{imp}}(\bar{\xi}, \bar{\xi}') &= \\ \text{Cov} \left[ m\ddot{e}(\theta, x_i) + d(\xi)\dot{e}(\theta, x_i) + k(\xi)e(\theta, x_i), \right. \\ \left. m\ddot{e}(\theta', x'_i) + d(\xi')\dot{e}(\theta', x'_i) + k(\xi')e(\theta', x'_i) \right] \end{aligned} \quad (12)$$

is more involved due to the correlation between the desired trajectory and its time derivatives. As differentiation is a linear operator,  $\dot{x}_d(\theta)$  and  $\ddot{x}_d(\theta)$  are also GPs with time derivative covariance

<sup>1</sup>Positivity is ensured by means of warped GPs [12]. In this case the GP priors are set as  $\log(d(\xi)) \sim \mathcal{GP}(\log \mu_d, k_d(\xi, \xi'))$  and  $\log k(\xi) \sim \mathcal{GP}(\log \mu_k, k_k(\xi, \xi'))$ .

<sup>2</sup>From (10) and (9), due to the products between impedance parameters and the desired trajectory,  $u_{\text{imp}}(\bar{\xi})$  involves non-central chi-squared terms.

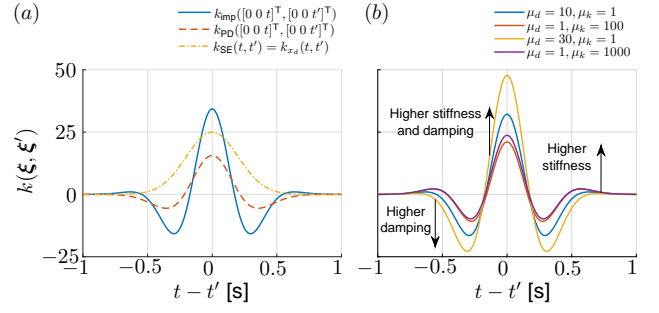


Fig. 1. (a) Covariance functions for a PD controller for the one-dimensional case with  $\theta = t$ ,  $x = x' = 0$ ,  $\dot{x} = \dot{x}' = 0$  and a SE kernel. The mean values for the mass, damping, stiffness and desired trajectory are set to  $\mu_m = 1$  kg,  $\mu_d = 10$  Ns/m,  $\mu_k = 100$  Nm and  $\mu_{x_d} = 0$  m. The hyperparameters for the damping, stiffness and desired trajectory SE covariance functions (16) are  $\{0.1, (0.1 \ 0.1)\}_d$ ,  $\{0.1, (0.1 \ 0.1)\}_k$  and  $\{0.1, (0.2)\}_{x_d}$  while the variance of the mass is  $\sigma_m^2 = 0.1$ . (b) Covariance functions for an impedance with identical parametrization as (a) but with different expected values for damping and stiffness.

functions [5]. From the properties of the covariance of sums  $\text{Cov}[\sum_r a_r X_r, \sum_s b_s Y_s] = \sum_{r,s} a_r b_s \text{Cov}[X_r, Y_s]$ , where  $X_r$  and  $Y_s$  are random variables and  $a_r$  and  $b_s$  are constants and considering the covariance of products [13], expression (12) involves the sum of covariances of all combination of product terms. For simple exposition, we first derive the covariance considering only the stiffness and damping terms, which, from a control perspective corresponds to a PD controller. The PD kernel is given by

$$\begin{aligned} k_{\text{PD}}(\xi, \xi') &= \text{Cov}[d(\xi)\dot{e}(\theta, x_i) + k(\xi)e(\theta, x_i), \\ &\quad d(\xi')\dot{e}(\theta', x'_i) + k(\xi')e(\theta', x'_i)] \\ &= \text{Cov}[k(\xi)e(\theta, x_i), k(\xi')e(\theta', x'_i)] \\ &\quad + \text{Cov}[k(\xi)e(\theta, x_i), d(\xi')\dot{e}(\theta', x'_i)] \\ &\quad + \text{Cov}[d(\xi)\dot{e}(\theta, x_i), k(\xi')e(\theta', x'_i)] \\ &\quad + \text{Cov}[d(\xi)\dot{e}(\theta, x_i), d(\xi')\dot{e}(\theta', x'_i)] \\ &= (\mu_k^2 + k_k(\xi, \xi'))k_{x_d}(\theta, \theta') \\ &\quad + (\mu_{x_d} - x_i)(\mu_{x_d} - x'_i)k_k(\xi, \xi') \\ &\quad + \mu_k \mu_d \left( \frac{\partial k_{x_d}(\theta, \theta')}{\partial t'} \right) + \mu_d \mu_k \left( \frac{\partial k_{x_d}(\theta, \theta')}{\partial t} \right) \\ &\quad + (\mu_d^2 + k_d(\xi, \xi')) \frac{\partial^2 k_{x_d}(\theta, \theta')}{\partial t \partial t'} \\ &\quad + (\dot{\mu}_{x_d} - \dot{x}_i)(\dot{\mu}_{x_d} - \dot{x}'_i)k_d(\xi, \xi'), \end{aligned} \quad (13)$$

where  $t$  and  $t'$  are the time stamps corresponding to observations  $\theta$  and  $\theta'$  respectively.

The full impedance kernel (12) yields

$$\begin{aligned} k_{\text{imp}}(\bar{\xi}, \bar{\xi}') &= k_{\text{PD}}(\xi, \xi') \\ &\quad + \mu_k \mu_m \left( \frac{\partial^2 k_{x_d}(\theta, \theta')}{\partial^2 t'} + \frac{\partial^2 k_{x_d}(\theta, \theta')}{\partial^2 t} \right) \\ &\quad + \mu_d \mu_m \left( \frac{\partial^3 k_{x_d}(\theta, \theta')}{\partial^2 t' \partial t} + \frac{\partial^3 k_{x_d}(\theta, \theta')}{\partial^2 t \partial t'} \right) \\ &\quad + (\mu_m^2 + \sigma_m^2) \frac{\partial^4 k_{x_d}(\theta, \theta')}{\partial^2 t \partial^2 t'} \\ &\quad + \sigma_m^2 (\dot{\mu}_{x_d} - \ddot{x}_i)(\dot{\mu}_{x_d} - \ddot{x}'_i). \end{aligned} \quad (14)$$

If  $\theta = t$  the computation of the time derivatives of covariance  $k_{x_d}(\theta, \theta')$  is straightforward. For any other parametrization, time derivatives are computed in terms of partial and time derivatives of  $\theta$  as

$$\begin{aligned}\frac{\partial k_{x_d}(\theta, \theta')}{\partial t'} &= \left( \frac{\partial k_{x_d}(\theta, \theta')}{\partial \theta'} \right)^\top \frac{\partial \theta'}{\partial t} \\ \frac{\partial^2 k_{x_d}(\theta, \theta')}{\partial t'^2} &= \left( \frac{\partial \theta'}{\partial t} \right)^\top \frac{\partial^2 k_{x_d}(\theta, \theta')}{\partial \theta'^2} \frac{\partial \theta'}{\partial t} \\ &\quad + \left( \frac{\partial k_{x_d}(\theta, \theta')}{\partial \theta'} \right)^\top \frac{\partial^2 \theta'}{\partial t^2}.\end{aligned}$$

Considering (10) and (8), the a priori statistical characterization of the interaction force is

$$u_{\text{int}}(\bar{\xi}) \sim \mathcal{GP} \left( \mathbb{E} [u_{\text{imp}}(\bar{\xi})], k_{\text{int}}(\bar{\xi}, \bar{\xi}') \right), \quad (15)$$

where

$$k_{\text{int}}(\bar{\xi}, \bar{\xi}') = k_{\text{imp}}(\bar{\xi}, \bar{\xi}') + k_{\hat{\text{int}}}(\bar{\xi}, \bar{\xi}') + \sigma_\tau^2.$$

For illustrative purposes, let all covariances for GP priors from (10) be Squared Exponential (SE) kernels

$$k_{\text{SE}}(z, z') = \sigma_f^2 \exp\{-(z - z')^\top \Lambda^{-1} (z - z')\}, \quad (16)$$

with hyperparameters  $\{\sigma_f^2, (l_1 \cdots l_n)\}_{\text{SE}}$ , where  $\sigma_f^2$  is the signal variance and  $\Lambda = \text{diag}(l_1 \cdots l_n)$  are the length scales for each input dimension. The SE kernel is infinitely differentiable and therefore valid for  $k_{x_d}(\theta, \theta')$ . It is the most widespread and applied kernel due to its smoothness and convergence properties [8].

The most relevant characteristic of the PD and the impedance kernels is the presence of terms comprising time derivatives of a latent desired trajectory. To depict the influence of this feature in correlations, Fig. 1 shows the covariance functions corresponding to a naïve SE kernel, a PD and an impedance kernel for a time-dependent desired trajectory. As depicted by the red dashed line the PD kernel considers the SE kernel derivative as an additive term that determines its profile. Similarly, the shape of the impedance kernel illustrated by the blue solid line is governed by the mass-related term that considers the second derivative of the SE kernel. The relevance of the stiffness, damping and mass terms are significantly influenced by their respective expected values.

Fig. 2 shows the covariance function for a one-dimensional configuration-dependent desired trajectory, i.e.  $\theta = x$ . When the velocity ( $\dot{\theta}$  is this case) of one of the input points is 0, the damping term is nullified as the tracking error derivative is also 0. Thus, the correlation is limited to the SE kernel of the stiffness term  $k(\xi)e(\theta, x_i)$  as depicted in Fig. 2(c) for  $\dot{x} = 0$ . When this is not the case correlations due to damping  $d(\xi)\dot{e}(\theta, x_i)$  arise. Fig. 2(d)(e) and Fig. 2(b), (a) show positive and negative values of  $\dot{x}$ , which determine the slope of the correlation around  $x - x' = 0$  as the derivative of the error trajectory is proportional to  $\dot{\theta}$ .

### C. Conditional distribution of latent functions

The probabilistic nature of the proposed model enables the computation of the conditional distribution of latent variables with priors (10). In the case of multivariate normality, conditional distributions are also Gaussian and computed in closed form. In our specific setting, the human desired trajectory  $x_d(\theta)$  is an especially relevant variable in many pHRI applications where an estimate of human intention is necessary. From (10) and (15), the joint distribution of a set of noisy observations of the interaction force  $\mathbf{y}_{\text{int}} = \{y_{\text{int},i}\}_{i=1}^h$  at input points  $\bar{\Xi} = \{\bar{\xi}_i\}_{i=1}^h$  and  $x_d(\theta_*)$  at test input  $\theta_*$  is

$$\mathcal{N} \left( \begin{bmatrix} \mathbf{y}_{\text{int}} \\ x_d(\theta_*) \end{bmatrix} \middle| \begin{bmatrix} \mathbb{E} [u_{\text{int}}(\bar{\Xi})] \\ \mu_{x_d} \end{bmatrix}, \begin{bmatrix} K_{\text{int}} & \text{Cov}[u_{\text{int}}(\bar{\Xi}), x_d(\theta_*)] \\ \text{Cov}[x_d(\theta_*), u_{\text{int}}(\bar{\Xi})] & k_{x_d}(\theta_*, \theta_*) \end{bmatrix} \right),$$

where  $K_{\text{int}} = k_{\text{int}}(\bar{\Xi}, \bar{\Xi}')$  and

$$\begin{aligned}\text{Cov}[u_{\text{int}}(\bar{\Xi}), x_d(\theta_*)] &= \text{Cov}[u_{\text{int}}(\bar{\Xi}), x_d(\theta_*)]^\top \\ &= \mu_k k_{x_d}(\Theta, \theta_*) + \mu_d \left( \frac{\partial k_{x_d}(\Theta, \theta_*)}{\partial t} \right) + \mu_m \left( \frac{\partial^2 k_{x_d}(\Theta, \theta_*)}{\partial t^2} \right),\end{aligned}$$

where  $\Theta = \{\theta_i\}_{i=1}^h$  are the desired trajectory inputs of  $\bar{\Xi}$ . The conditional distribution follows applying Bayes' rule, yielding

$$P(x_d(\theta) | u_{\text{int}}(\bar{\xi})) = \mathcal{N}(x_d(\theta_*) | \mathbb{E}[x_d(\theta_*)], \text{Var}[x_d(\theta_*)]), \quad (17)$$

where

$$\begin{aligned}\mathbb{E}[x_d(\theta_*)] &= \mu_{x_d} \\ &\quad + \text{Cov}[u_{\text{int}}(\bar{\Xi}), x_d(\theta_*)] K_{\text{int}}^{-1} (\mathbf{y}_{\text{int}} - \mathbb{E}[u_{\text{int}}(\bar{\Xi})])\end{aligned}$$

and

$$\begin{aligned}\text{Var}[x_d(\theta_*)] &= k_{x_d}(\theta_*, \theta_*) \\ &\quad + \text{Cov}[u_{\text{int}}(\bar{\Xi}), x_d(\theta_*)] K_{\text{int}}^{-1} \text{Cov}[x_d(\theta_*), u_{\text{int}}(\bar{\Xi})].\end{aligned}$$

The computation of conditional distributions over other latent functionals such as the stiffness  $k(\xi)$  or damping  $d(\xi)$  is similar.

Choosing a suitable prior for  $x_d(\theta)$  is also essential as all impedance parameters depend on it. Depending on the task and the application we may parametrize it as a function of time or as a function of other task variables and their time derivatives. An interesting alternative considers a priori

$$x_d(x_i, \theta) \sim \mathcal{GP}(x_i, k_{x_d}(\theta, \theta')), \quad (18)$$

i.e., the human is in equilibrium and therefore, from (11) and (15)  $\mathbb{E}[u_{\text{int}}(\bar{\xi})] = 0$ . This is suitable for modeling tasks where no information about the task is available a priori.

## V. EVALUATION

In order to validate the impedance-based GP model, we analyzed its prediction performance in an experiment with real human users. In our evaluations, all GP priors (10) have SE covariance functions (16). The prediction performance evaluated using the standardized mean squared error (SMSE)

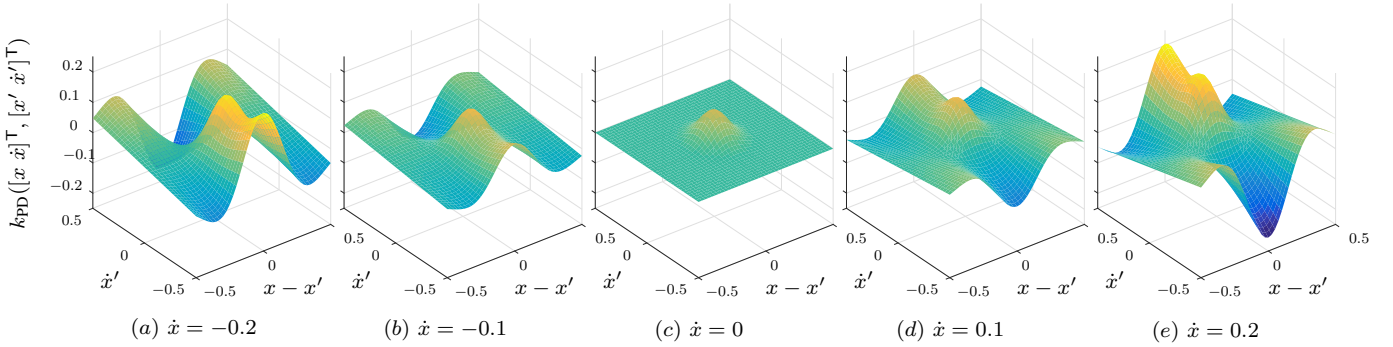


Fig. 2. Covariance function for one-dimensional case of a PD controller (13) with a configuration-dependent error trajectory  $\theta = x$  and Squared Exponential (SE) kernels with hyperparameters  $\{0.1, (0.1 \ 0.1)\}_d$ ,  $\{0.1, (0.1 \ 0.1)\}_k$  and  $\{1, (0.2)\}_{x_d}$  for damping, stiffness and an error trajectory respectively. The expected damping and stiffness are set to  $\mu_d = 1.5$  Ns/m and  $\mu_k = 1$  Nm with  $\mu_{x_d} = 0$  m.

and the mean standardized log loss (MSLL). In SMSE, the squared residuals are normalized with the variance of the test outputs. On the other hand, in MSLL, the mean negative log probability minus the log probability of a naïve Gaussian with the mean and variance given by the training points [14].

In order to validate the impedance-based GP model, we analyzed its prediction performance in a simulated model of a human arm and in an experiment with real human users.

#### A. Simulated human arm

We simulated a two-link arm trajectory based on the neuromechanical arm model reported in [15] using *Matlab*. This model was selected as it is structurally more complex than our GP model, and it derives a 2D trajectory from simulated muscle activities, providing a physiologically plausible impedance definition. The model simulated the muscle tension  $u_m$  for attaining a desired trajectory as

$$u_m = K_\lambda(e_\lambda) + D_\lambda(\dot{e}_\lambda) \\ K_\lambda = K_0 + K_1 u_{\text{CNS}} \quad D_\lambda = 1/12 K_\lambda,$$

where  $K_\lambda, D_\lambda, e_\lambda$  indicate the stiffness, damping and error at the muscular level,  $u_{\text{CNS}}$  is the neural control signal and  $K_0$  and  $K_1$  are constant and activation-dependent stiffness terms, respectively. A reference trajectory was designed as a 0.04 m radius circle joint with 4 arcs subtending 270 degrees attached laterally and vertically to a central circle (Fig. 5). The same trajectory was prescribed 3 times without interruption at a rate of 2.618 rad/s to form a single trial. We simulated two different stiffness profiles at 500 Hz. For low-stiffness simulation,  $K_0$  was set to 3360 as of [15]. For high-stiffness simulation,  $K_0$  was set to 16800. For both simulations  $K_1 = 0.035K_0$ . The average simulated hand stiffness and damping are shown in Table I. We consider the model (15) for a configuration-dependent

TABLE I

Average (standard deviation) stiffness and damping at the end-effector from the simulation.

simulation type	damping ([Ns/m])		stiffness [N/m]	
	x	y	x	y
high-stiffness	48.07 (6.20)	60.29 (7.55)	576.8 (74.4)	723.5 (90.6)
low-stiffness	9.89(1.47)	12.4 (.73)	118.7 (17.6)	148.4 (20.7)

desired trajectory  $\theta = x$  with a priori equilibrium assumption (18). We assume all impedance parameters constant and deterministic. We compare this model with a naïve GP prior  $u_{\text{int}}(\xi) \sim \mathcal{GP}(0, k_{\text{SE}}(\xi, \xi'))$ . The training set is given by the simulated trajectories downsampled to 0.2Hz, and the test inputs are the full trajectories.

We train the naïve model hyperparameters and set identical hyperparameters for  $\hat{u}_{\text{int}}(\xi)$  in (15). In addition, the expected mass is set to  $\mu_m = 3$  kg and the desired trajectory kernel has hyperparameters  $\{10^{-6}, (0.2 \ 0.2)\}_{x_d}$  and  $\sigma_\tau^2 = 10^{-4}$ .

The prediction performance for different values of  $\mu_k$  and  $\mu_d$  to the naïve model are shown in Fig. 3. The SMSE for the low stiffness simulation shows increased performance to the naïve model for low stiffness and damping, corresponding to the simulated values shown in Table I. High stiffness and damping values significantly decreases performance. However, in terms of the MSLL, which considers uncertainty, the prediction performance increases throughout the whole stiffness and damping range. The results for the high stiffness simulation show marginally improved performance. The minimum error is achieved for stiffness in the mid range and with a damping parameter, in accordance with the simulated values. A similar dependency is found in terms of the MSLL.

Fig. 4 shows how the proposed model infers the latent desired trajectory, computed in (17), in terms of the difference with the state for different stiffness and damping values considering the full high stiffness simulation. The high stiffness model depicted by the red arrows expects low deviations and higher tracking accuracy, thus the state being close to the desired trajectory. In contrast, the low stiffness model illustrated by the green arrows infers higher deviations as it assumes lower tracking accuracy.

#### B. Experiment with humans

To assess prediction performance with human data and envisaging real applications for robot control, we designed an experiment with human users with emphasis on sparse approximations.

1) *Experimental setup*: The haptic interface (Fig. 5) consists of a two degrees-of-freedom (anteroposterior and mediolateral plane of the user standing in front) linear-actuated device (*ThrustTube*) with a free-spinning handle (su-

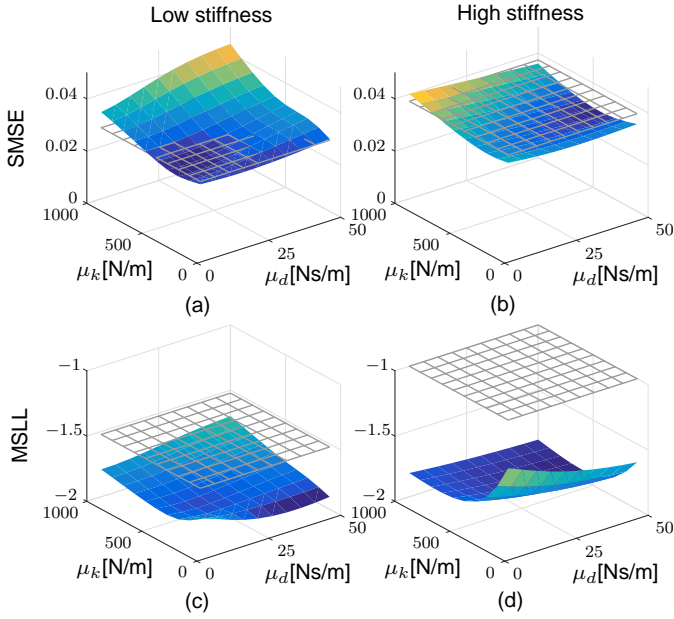


Fig. 3. Prediction performance quantified by standardized mean square error (SMSE) and mean standardized log loss (MSLL) for the configuration-dependent model  $\theta = t$ . The grey grid represents the performance of the naïve GP model.

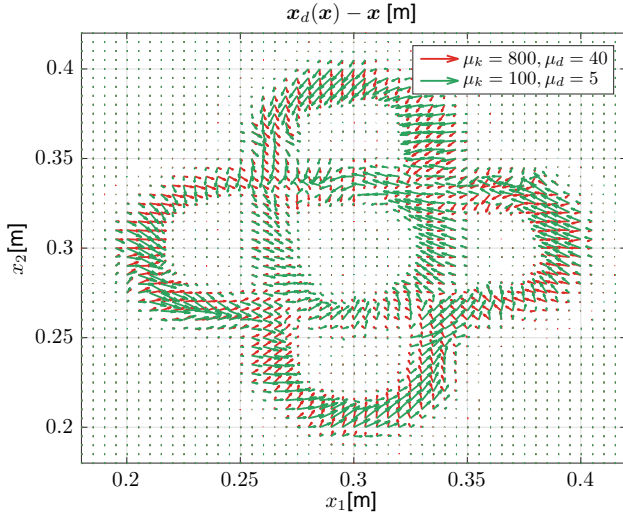


Fig. 4. Desired trajectory reconstruction in terms of the difference with the state  $x_d(x) - x$  for the state-dependent model  $\theta = x$  for the high stiffness simulation.

peroinferior direction of the user) at the grasp point. Each actuator is equipped with a position encoder with precision of  $1 \mu\text{m}$ . Attached to the handle is a 6 DoF force/torque sensor (*JR3*), which measures the human force input. The workspace of the experimental device is  $(-0.15, 0.15)$  m for each dimension. A virtual scene is visually represented on a display on top of the device to task description serving as a guide for performing the task. To enable haptic interaction with the user, the robot follows an admittance control scheme

$$M_r \ddot{x} + D_r \dot{x} = u_{\text{int}}$$

with  $M_r = \text{diag}\{2, 2\}$  kg and  $D_r = \text{diag}\{6, 6\}$  Nm/s, implemented in *Matlab's Simulink Coder* and executed on

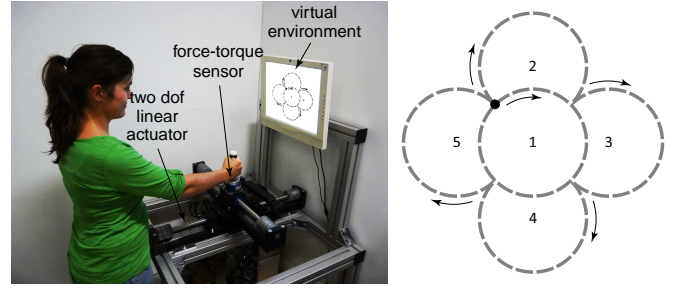


Fig. 5. Experimental setup and a tracking path. A participant grasped a handle on a two DoF linear actuator with force/torque sensor and reproduced a path with a flower shape as displayed on the monitor in front. Starting at the black dot, the arrows and numbers respectively describe the direction and order of the motion.

*Linux Preempt/RT* at a sampling rate of 1 kHz running on an external PC.

To robot implements an admittance control scheme

$$M_r \ddot{x} + D_r \dot{x} = u_{\text{int}}$$

with  $M_r = \text{diag}\{2, 2\}$  kg and  $D_r = \text{diag}\{6, 6\}$  Nm/s. We let 3 different subjects (all male, average age 26) perform the task repeated cyclically 10 times with no pauses. The subjects had the opportunity to familiarize with the haptic device for a few minutes before the experiment and were told to follow the pre-defined trajectory for the given repetitions.

As the computational complexity of (7) hinders the application of GPs to large datasets, we implement a local GP approximation [16], which partition the input space into several local models. We follow [17], where predictions  $y_*(z)$  are computed as an average weighted sum of  $L$  local GPs

$$y_*(z) = \frac{\sum_{l=1}^L k(z, z_l) y_{*l}(z)}{\sum_{l=1}^L k(z, z_l)},$$

where  $z_l$  and  $y_{*l}$  are the center and the prediction of the  $l$ -th local GP, respectively. In order to ensure a constant computation time, we consider that the input-space is bounded by the operational constraints of the human arm and a partitioning is possible a priori<sup>3</sup>. This enables the definition of each cluster as a sparse GP [18], ensuring fast predictions. For each incoming observation every local model is updated efficiently by means of the methods described in [19]. Assuming that each local sparse GP has  $B$  inducing inputs, the complexity of online updates and predictions is reduced to  $\mathcal{O}(LB^2)$ .

We evaluate model (15) with  $\theta = [x^T \dot{x}^T]^T$  and a priori equilibrium assumption (18). For computational tractability, we restrict the model to position and velocity inputs, setting acceleration and jerk arising in the covariance of (15) to  $\mathbf{0}$ . We compare this model with a naïve GP prior  $u_{\text{int}}(\xi) \sim \mathcal{GP}(0, k_{\text{SE}}(\xi, \xi'))$ . We train the naïve model hyperparameters [16] with the first repetition of each user

<sup>3</sup>If this is not the case, several methods address this issue by incrementally building data clusters, e.g., [17].

and we set identical hyperparameters for  $\hat{u}_{\text{int},\varepsilon}(\bar{\xi})$ . The expected impedance parameters to  $\mu_m = 3$  kg,  $\mu_d = 15$  Ns/m and  $\mu_k = 300$  N/m. Damping and stiffness covariance functions are set to  $\{50^2, (0.1 \ 0.1 \ 0.3 \ 0.3)\}_k$  and  $\{5^2, (0.1 \ 0.1 \ 0.3 \ 0.3)\}_d$ , the desired trajectory kernel has hyperparameters  $\{10^{-4}, (0.05 \ 0.05 \ 0.3 \ 0.3)\}_{x_d}$  and  $\sigma_\tau^2 = 10^{-4}$ .

In our local sparse implementation, we set a total of  $5 \times 5$  local models distributed as a grid covering the robot workspace. Each local model is composed of  $(3 \times 3) \times (3 \times 3)$  basis vectors distributed as a grid in position and velocity space, respectively. Velocities are assumed to be in the range  $(-0.12, 0.12)$  m/s due to task constraints. To assess prediction performance, we evaluate the SMSE of the captured dataset for two conditions. In condition (A) we update the model posterior online for every observed data point. In condition (B), we update the model only during the first of the 10 task repetitions.

2) *Experimental Results:* The experimental results are shown in Table II. The improvement of the model was more prominent in condition (A) with though the superior performance of the impedance-based model was also observed in condition (B). Despite the fact that the improvement seems small in value, under sparsity, the inclusion of the impedance structure increases accuracy.

TABLE II  
SMSE for both experimental conditions.

	(A)	(B)
Impedance-based model (15)	0.08	0.10
naïve SE kernel (16)	0.11	0.13

In summary, the proposed impedance-based GP model predicts human behavior with more fidelity than a naïve GP model. In addition, it provides an estimate of the assumed human-desired trajectory with confidence levels. However, results also depict a dependency between the model’s performance and the assumed priors for the impedance parameters and the latent desired trajectory, which requires a care in selection.

## VI. CONCLUSION

We presented an impedance-based GP model for predicting human arm behavior during physical interaction with a haptic device which incorporated empirically supported human sensory-motor control to exploit the flexibility of GPs. By assuming a GP prior on the latent desired trajectory and the human arm impedance parameters, we derive the correlation functions of an impedance-like control structure that efficiently represents human behavior. The results show the benefit performance of the human-based GP model, demonstrating superior performance with regard to a naïve GP model. However, the prediction performance depends

on an appropriate selection of the priors of the impedance parameters. These insights suggest the potential benefits for a system identification concerning underlying human sensory-motor processes and control for pHRI are concurrently executed through a integrated approach as a future work.

## ACKNOWLEDGMENTS

This research is partly supported by the ERC Starting Grant “Control based on Human Models (con-humo)” under grant agreement 337654 and by the European Union’s Horizon 2020 research and innovation programme under grant agreement No 643433, project Robotic Assistant for MCI Patients at home (RAMCIP)”.

## REFERENCES

- [1] S. Calinon, P. Evrard, E. Gribovskaya, A. Billard, and A. Kheddar, “Learning collaborative manipulation tasks by demonstration using a haptic interface,” in *Proc. ICAR*, 2009, pp. 1–6.
- [2] A. Billard, S. Calinon, R. Dillmann, and S. Schaal, “Robot Programming by Demonstration,” in *Handbook of Robotics*, B. Siciliano and O. Khatib, Eds. Springer, 2008, pp. 1371–1394.
- [3] E. Gribovskaya, A. Kheddar, and A. Billard, “Motion Learning and Adaptive Impedance for Robot Control during Physical Interaction with Humans,” in *Proc. IEEE ICRA*, 2011, pp. 4326–4332.
- [4] J. Medina, D. Lee, and S. Hirche, “Risk Sensitive Optimal Feedback Control for Haptic Assistance,” in *Proc. IEEE ICRA*, 2012.
- [5] E. Solak, R. Murray-Smith, W. E. Leithead, D. J. Leith, and C. E. Rasmussen, “Derivative observations in gaussian process models of dynamic systems,” 2003.
- [6] J. Kocijan, A. Girard, B. Banko, and R. Murray-Smith, “Dynamic Systems Identification with Gaussian Processes,” *Mathematical and Computer Modelling of Dynamical Systems*, vol. 11, no. 4, pp. 411–424, 2005.
- [7] M. Alvarez, D. Luengo, and N. Lawrence, “Linear Latent Force Models Using Gaussian Processes,” *IEEE Trans. Pattern Anal. Mach. Intell.*, vol. 35, no. 11, pp. 2693–2705, 2013.
- [8] A. Van Der Vaart and H. Van Zanten, “Information rates of nonparametric gaussian process methods,” *The Journal of Machine Learning Research*, vol. 12, pp. 2095–2119, 2011.
- [9] H. Gomi and R. Osu, “Task-dependent viscoelasticity of human multijoint arm and its spatial characteristics for interaction with environments,” *J. Neurosci.*, vol. 18, no. 21, pp. 8965–78, Nov. 1998.
- [10] J. Mizrahi, “Mechanical Impedance and Its Relations to Motor Control, Limb Dynamics, and Motion Biomechanics,” *J. Med. Biol. Eng.*, vol. 35, no. 1, pp. 1–20, 2015.
- [11] M. Kawato, “Internal models for motor control and trajectory planning,” *Curr. Opin. Neurobiol.*, vol. 9, no. 6, pp. 718–727, Dec. 1999.
- [12] E. Snelson, C. E. Rasmussen, and Z. Ghahramani, “Warped gaussian processes,” *Advances in neural information processing systems*, vol. 16, pp. 337–344, 2004.
- [13] G. W. Bohrnstedt and A. S. Goldberger, “On the exact covariance of products of random variables,” *Journal of the American Statistical Association*, vol. 64, no. 328, pp. 1439–1442, 1969.
- [14] C. E. Rasmussen, “Gaussian processes for machine learning,” 2006.
- [15] D. W. Franklin, E. Burdet, K. P. Tee, R. Osu, C.-M. Chew, T. E. Milner, and M. Kawato, “CNS learns stable, accurate, and efficient movements using a simple algorithm,” *J. Neurosci.*, vol. 28, no. 44, pp. 11 165–11 173, 2008.
- [16] E. Snelson and Z. Ghahramani, “Local and global sparse gaussian process approximations,” in *Proc. AISTATS*, 2007, pp. 524–531.
- [17] D. Nguyen-Tuong, M. Seeger, and J. Peters, “Real-time local gp model learning,” in *From Motor Learning to Interaction Learning in Robots*. Springer, 2010, pp. 193–207.
- [18] E. Snelson and Z. Ghahramani, “Sparse gaussian processes using pseudo-inputs,” 2006.
- [19] S. V. Vaerenbergh, M. Lázaro-Gredilla, and I. Santamaría, “Kernel recursive least-squares tracker for time-varying regression,” *IEEE Trans. Neural Netw. Learn. Syst.*, vol. 23, no. 8, pp. 1313–1326, 2012.